ARTICLE NO. 78-821R

Degradation of a Laser Beam by a Two-Dimensional Turbulent Jet

G. F. Cudahy,* J. T. Van Kuren†
Air Force Flight Dynamics Laboratory, Wright-Patterson AFB, Ohio
and
H. E. Wright‡
Air Force Institute of Technology, Wright-Patterson AFB, Ohio

A laser beam traversing turbulence undergoes an intensity reduction which is correlated with the statistical behavior of refractive index perturbations. The analytical relation predicts degradation as a function of beam diameter, path length, wave number, and wave structure function. Refractive index perturbations are approximated via the equations of state, using temperature and velocity perturbations. An experiment was conducted in which visible wavelength lasers traversed a well-documented, two-dimensional jet. Temperature perturbations vary from 0.25 to 1.89 K, and velocity fluctuations range from 9.2 to 30.8 m/s. Measured central spot intensities are as low as 18% of the undisturbed beam, depending on jet Mach number, beam position relative to the jet exit, and wavelength. The average difference between theory and experiment is 2% in terms of far-field intensity.

Nomenclature

B = correlation function
C = constant
F = focal length of far-field forming lens
I = laser beam intensity
J_0 = Bessel function of the first kind of order zero
k = wave number of the laser beam
L = beam path length through turbulence
L_0 = turbulence outer scale or integral scale
m = correction constant in temperature correlation
N = refractive index perturbations
P = pressure
R = input beam radius
r = optical radius in the near field
S = optical radius at which the Gaussian input beam is truncated
s = optical radius in the far field
T = modulation transfer function (MTF)
U = velocity
x = coordinate in the direction of the jet
y = coordinate in the direction of the laser beam
z = coordinate normal to beam and jet
λ = wavelength
ρ = density
Θ = temperature

Subscripts

d = relative to input beam diameter
i = finite-difference index
lens = far-field forming lens
m,q = variable indices
n = index of refraction
o = turbulence or unperturbed value; or relative to initial jet size
p = pressure
u = velocity
Θ = temperature
Θ_s = measured value
τ = turbulence refractive index
$1,2$ = time indices

Presented as Paper 78-821 at the AIAA 10th Aerodynamics Testing Conference, San Diego, Calif., April 19-21, 1978; submitted July 7, 1978; revision received Feb. 12, 1979.

Index categories: Lasers; Jets, Wakes, and Viscid-Inviscid Flow Interactions.

*Col., USAF; Commander, AFFDL. Member AIAA.
†Aerospace Engineer. Associate Fellow AIAA.
‡Associate Professor. Member AIAA.

I. Introduction

THE effect that the turbulent flowfield of a high subsonic Mach number, two-dimensional jet shear layer produces on a coherent light beam has not been quantified. The refractive index perturbations cause a decrease in the central spot intensity of the beam in the far field because the total energy is spread over a larger area than in the unperturbated case. Furthermore, the long-time average at the mean location of the central spot is decreased by beam wandering. Numerous theoretical and experimental efforts have been presented concerning the propagation of laser beams through natural atmospheric turbulence; however, in the atmosphere, the absolute intensities of the velocity, temperature, and pressure perturbations are relatively low, the beam path lengths are usually long, and the turbulence scales are quite large compared to beam diameter.[1-6] Recently, lasers have been used for wind tunnel diagnostics and in certain applications involving propagation out of aircraft, in which case the beams must pass through boundary layers and free shear layers where the turbulence scales are the same order as the beam size.

The present study was an attempt to provide a controlled, well-documented turbulence field and to correlate the degradation of the far-field central spot intensity formed by a collimated coherent light beam traversing the high-intensity turbulence of a shear layer. In addition, an attempt was made to measure the spreading of the energy over a larger area in the far field (termed broadening), and the motion of the beam in the far field (called wandering).

A two-dimensional jet with a well-designed stilling chamber and subsonic nozzle was fabricated. This setup also provided

double shear layers for added sensitivity. The uniform velocity coreflow could be varied with Mach numbers ranging from 0.4 to 0.8 to emphasize the compressible regime. To determine if wavelength and beam size relative to turbulence scale were important, two laser frequencies were used and three beam sizes were used at each frequency. The beam traversed the turbulent jet successively at 25, 50, and 75 nozzle widths downstream from the nozzle exit.

II. Theoretical Considerations

The purpose of this study is to determine the far-field central spot reduction in intensity caused by the turbulence-induced refractive index perturbations through which the laser-generated Gaussian plane wave propagates. For homogeneous, isotropic turbulence, the transformation of the laser beam from the area of turbulence perturbations to the observation point in the far field can be described by:

$$I(s) = C\int_{\theta}^{S} T_{\text{lens}}(r)\, T_{\tau}(r)\, T_{d}(r)\, J_0\left(\frac{2\pi sr}{F\lambda}\right) r\,dr \tag{1}$$

The far-field forming lens MTF reduces to approximate unity if the lens diameter is larger than the truncated beam diameter and the far field is observed in the focal plane of the lens. Equation (1) is a Hankel transformation which derives from a Fourier transformation when the function to be transformed has circular symmetry.

The cylindrical coordinates r and s are perpendicular to the y axis, which lies on the center of the laser beam and is positive in the direction of the beam propagation. The x axis has its origin on the center of the beam, and is positive in the direction of the airflow exhausting from the nozzle. The z axis is normal to the beam and the jet.

A correlation function is defined as:

$$B_{mq}(r,y) \equiv \langle m(\bar{r}_1,\bar{y}_1)\, q(\bar{r}_2,\bar{y}_2)\rangle \tag{2}$$

and is the statistical measure of the interdependence of the variables being correlated.

Owens[7] shows that the refractive index for dry air and 5327 Å light is:

$$N \simeq 1 + (79.0\times 10^{-6})\,(P/\Theta) \tag{3}$$

where P is the pressure in millibars and Θ is the temperature in Kelvin.

Elimination of the steady-state portion of Eq. (3) and dropping of the second-order terms yields

$$n = (79.0\times 10^{-6})\left(\frac{P}{\bar{\Theta}} - \frac{\bar{P}\Theta}{\bar{\Theta}^2}\right) \tag{4}$$

For homogeneous, isotropic turbulence, the refractive index correlation function can now be described in terms of the turbulence pressure and temperature perturbations.

$$B_n(r) \simeq (79.0\times 10^{-6})^2\left[\frac{B_p(r)}{\bar{\Theta}^2} + \frac{\bar{P}^2}{\bar{\Theta}^4} B_{\theta}(r)\right] \tag{5}$$

As a result of heuristic arguments, it is assumed that

$$\frac{2\bar{P}}{\bar{\Theta}^3} B_{p\theta}(r) \ll \frac{B_p(r)}{\bar{\Theta}^2} + \frac{\bar{P}^2}{\bar{\Theta}^4} B_{\theta}(r) \tag{6}$$

and that $B_p(r)$ and $B_{\Theta}(r)$ are of the same order.

The assumed relationship between pressure perturbations and velocity perturbations, based on results of several authors,[8] is

$$B_p(r) = (\rho^2/2)\, B_u(r)^2 \tag{7}$$

The ability to measure accurately the high-frequency temperature perturbations also proves to be difficult. Analysis show the mild dependence of the frequency response of a thin finite length unheated wire upon mean velocity. It also shows that the frequency response of a typical wire probe is insufficient to measure the small-size eddies expected in the type of flow used in this investigation. A method was developed to correct the temperature correlation function, which is obtained with a temperature sensor of inadequate frequency response. The correction is based on two concepts. The first is that the normalized temperature and velocity correlation functions at the same point in space in the same homogeneous flowfield are almost identical.[9,6]

The second concept is that the correlation function at large r has complete dependence upon the flowfield eddies with wavelengths larger than r.[9] Using the two concepts, a correction to the measured correlation function was developed.

$$B_{\theta}(r) = mB_{\theta s}(0)\,\hat{B}_u(r) \tag{8}$$

Now, the final form of the turbulence MTF, which was used in this study, can be presented.

$$T_{\tau} = \exp\left[-4k^2 L\int_0^{\infty}[B_n(y) - B_n(\sqrt{r^2+y^2})]\,dy\right] \tag{9}$$

Substituion of Eqs. (5) and (7) into Eq. (9) yields, for smoothly varying turbulence characteristics in the direction of beam propagation, where N layers of homogeneous turbulence are assumed,

$$T_{\tau} = \exp\left[-4k^2(79\times 10^{-6})^2 \sum_{i=1}^{N}\left[\frac{\Delta L_i}{\bar{\Theta}_i^4}\int_0^{\infty}\left\{\frac{\rho_i^2\bar{\Theta}_i^2}{2}[B_{ui}^2(y) - B_{ui}^2(\sqrt{r^2+y^2})] + \bar{P}_i^2[B_{\theta i}(y) - B_{\theta i}(\sqrt{r^2+y^2})]\right\}dy\right]\right] \tag{10}$$

In order to find the modulation transfer function of the unperturbed beam intensity, the unperturbed beam amplitude is transformed into the observation plane, that is, the far field. The unperturbed beams prior to the turbulence field are Gaussian plane waves, whose amplitude is symmetrical about the y axis. The input beam modulation transfer function T_D has been shown in Ref. 8.

The modulation transfer functions for the turbulence-induced refractive index perturbations, as determined by Eq. (10), is a statistical quantity, in that the time of measurement of the velocity and temperature perturbations is large as compared to the time scale of the turbulence, $L_0/\bar{U}$.[10] The far-field intensity, as determined by Eq. (1), when using these statistical quantities for the turbulence MTF is, therefore, an average intensity. If the perturbed intensity is normalized by the unperturbed central spot intensity, and the lens and beam amplitude MTFs are substituted into Eq. (1),

$$\frac{I(s)}{I_0(0)} = \hat{I}(s) = \left[\int_0^S e^{-r^2/2R^2} T_{\tau} J_0\left(\frac{2\pi rs}{F\lambda}\right) r\,dr\right] \Big/ \left[\int_0^S e^{-r^2/2R^2} r\,dr\right] \tag{11}$$

If, as in this investigation, the far-field central spot intensity is the variable of interest, Eq. (11) becomes $\hat{I}(0)$.

III. Experiments

Laser Beam Generation

The lasers used were the Spectra Physics Model 124A with Model 255 Exciter, which is a 15 mW He-Ne laser with a 6328

Table 1 Test conditions

Mach number	0.4	0.6	0.8
Test station, cm	25	50	75
Wavelength, Å		6328	4416
Beam size, $2R$ (mm)	50.0	26.0	12.3

Å output, and a Spectra Physics Model 185 with Model 285 Exciter, which is a He-Cd laser with a 4416 Å output. The beam-forming telescope attached to the output port of each laser was a Spectra Physics Model 336 collimating lens utilizing Spectra Physics Model 332 spatial filters. The expanding lenses and spatial filters were chosen to yield approximate Gaussian beams of diameters shown in Table 1.

Far-Field Measurements

Figure 1 shows the physical layout of the far-field forming and detection equipment. The far field was formed in the focal plane of a lens which was considerably larger than the largest laser beam tested. The far field was observed by means of a microscope objective projecting the far-field image onto an opal glass. A modified television camera viewed the image on the opal glass and the output of the camera was viewed on an oscilloscope. A digital counter was used to provide external synchronization to the oscilloscope, such that the amplitude of any desired horizontal line or groups of horizontal lines may be viewed. These amplitudes were recorded with a polaroid camera.

The recording of the perturbed beam's far-field spot in a very short time, in order to separate degradation due to beam broadening from that due to beam wandering, was one of the goals of the experiment. If the videcon could be single-line scanned, the laser beam integration time on the target could be greatly reduced, thus reducing the persistence of the image of the laser beam on the target. This would then increase the frequency response of the laser beam measuring capability. The silicon target videcon could be single-line scanned without significantly degrading the videcon output; thus, the silicon target videcon was chosen to be the laser beam far-field spot detection device.

Several prerequisites were imposed on the turbulent refractive index field to be generated. The turbulence had to be classical, precisely duplicatable from test to test, fairly uniform across the laser beam, vary smoothly in the direction of laser beam propagation, and have no physical surfaces in the immediate vicinity of the turbulent field through which the beam would have to propagate. This led to the choice of a free jet issuing into quiescent room air. The free jet is well documented analytically and experimentally.[9,11]

Free Jet Nozzle

The constraint of uniformity across the laser beam in planes perpendicular to the direction of propagation is most closely satisified by a plane free jet. A 1×10 cm knife-edge nozzle was chosen to provide an approximation to a plane free jet. The nozzle was symmetrically convergent to the exit, except that the last 1 cm of the nozzle inside face is parallel to the x direction. The transitions from the convergent sections to the exit faces were well rounded. At 25, 50, and 75 nozzle widths downstream from the nozzle exit, the laser beam turbulent field path lengths are approximately 10, 20, and 30 cm, respectively, and, at these locations, the turbulence field is fully developed.

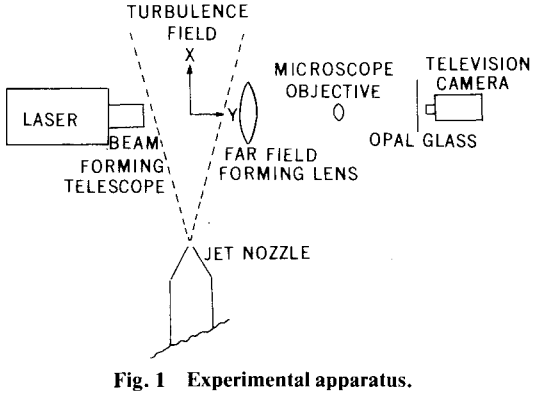

Fig. 1 Experimental apparatus.

The desire to trace the turbulent field origin to the shear layer caused by the freejet issuing into quiescent laboratory air dictated laminar flow in the nozzle exhaust plane. Also, most freejet theories assume that the nozzle exit velocity is uniform. Therefore, the nozzle exit velocity design specifications required a turbulence intensity of less than 1% and a uniform mean velocity across the entire exhaust plane.

Two basic requirements for the turbulence measuring equipment were established—one was to determine whether the turbulence was well defined and repeatable, and the other was to obtain the turbulence information required to fulfill the demands of this experiment.

The primary instrumentation for the turbulence measurements was a Thermo-Systems, Inc., (TSI) anemometer system using fine wire sensors and associated equipment.

TSI Model 1050 anemometers were used to process signals from the fine wire sensors during calibration and data collection. For velocity measurements, both mean and perturbations, the anemometers were operated in the constant temperature mode with their electrical circuits optimized for maximum frequency response. The sensors were operated at a temperature several hundred degrees above the flow mean temperature in order to achieve maximum sensitivity to velocity perturbations. For temperature perturbation measurements, only one sensor and one anemometer was used and the anemometer was operated in the constant-current mode with a very small sensing current flowing in the wire sensor; thus, the sensor temperature followed the temperature of the fluid.

Sensors 4 μ in diameter were selected, since they were readily available and gave acceptable frequency response for velocity measurements. However, they did not give a completely acceptable frequency response for measuring temperature perturbations.

Using the constant temperature anemometry system, including single-wire sensor and linearizer with proper coefficients, the jet nozzle exit flow was examined at the three exit velocities selected for this study in order to determine uniformity of the velocity, time variance of velocity, turbulence intensity, and velocity measured vs calculated from total conditions. The exit velocity was very nearly constant across the nozzle exit plane. The boundary layer was less than 0.2 mm thick. The turbulence intensity was less than 0.3%; that is, the rms turbulence velocity was less than 0.3% of the mean flow velocity for all exit velocities examined. The 0.3% value was established as the measuring system limitation due to electronic noise.

Next, the jet core and turbulence field were examined using the constant temperature anemometry system. The jet was symmetrical in the vertical and horizontal directions about the x axis. The maximum mean velocity occurred along the x axis. The spread of the jet calculated by taking $\bar{U}_{loc}/\bar{U}_{cen} = 1/2$ shows a half-angle of 5.0 deg, as compared to predicted values of 6.5 deg for a plane jet and 5.0 deg for a round jet.

Figure 2 shows the nondimensionalized mean velocities at 25, 50, and 75 jet nozzle widths downstream from the nozzle exit. Here $Y_{1/2}$ is the point at each test station where $U_{loc} = 1/2 U_{cen}$ and is used to nondimensionalize the measurement distance from the x axis in the y direction and U_{cen} is the velocity on the centerline, and is the nondimensionalizing parameter. Figure 2 shows that the flow

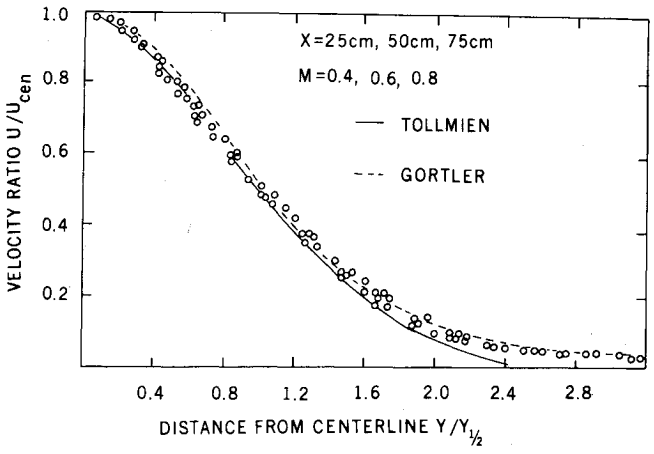

Fig. 2 Velocity similarity.

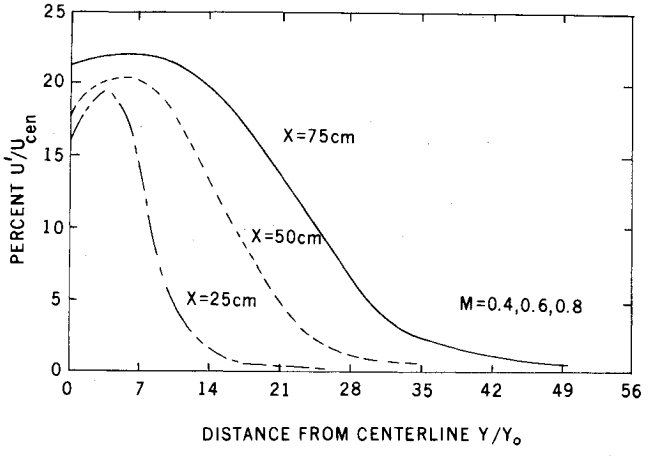

Fig. 3 Turbulence intensity profiles.

mean velocities were similar and agreed closely with the theoretical values of Gortler and Tollmien.

The nondimensionalized turbulence intensity profiles for all three test planes and test velocities are shown in Fig. 3. The turbulence intensities were similar in each test plane, and the point of maximum intensity spreads at half angle of approximately 3 deg in the direction of the jet flow. Additional information about the flowfield generated by the nozzle used in this experiment can be obtained from Ref. 11.

Initially, the Spectra Physics Model 336 collimating lens, together with the Specta Physics Model 332 spatial filters, was adjusted to give a symmetrical beam with maximum central spot intensity as measured by a Spectra Physics 401C power meter. The power meter was equipped with a small aperture and was scanned across the beam close to the exit of the collimating lens to insure symmetry and also to determine the points at which the central spot intensity value was reduced by exp(−2). The beam diameter was defined as the distance between two diagonally opposed points at which the maximum intensity was reduced by exp(−2).

IV. Results

Turbulence Characteristics Used to Predict Laser Beam Degradation

The refractive index perturbations, which have the major effect on the laser beam degradation of this investigation, were caused by turbulence-induced density variations in the active medium through which the laser beam propagates. These density variations were not amenable to direct measurement; thus, the equation of state was used to determine turbulent density variations via other readily measurable turbulence quantities. It was determined that

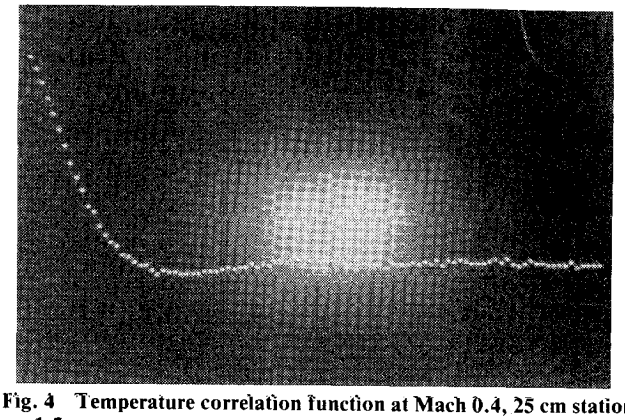

Fig. 4 Temperature correlation function at Mach 0.4, 25 cm station, $y = 1.5$ cm.

velocity and temperature perturbations could be transformed into density and, subsequently, refractive index perturbations. Since the frequency response of the temperature measuring device was insufficient for the temperature field to be measured, a method was developed to correct the temperature measurements obtained with this device.

The measurement and recording of instantaneous turbulent flowfield characteristics for the entire flowfield area of interest for a given experimental configuration of investigation were not possible. Statistical characterization of the turbulent flowfield was, therefore, resorted to, and the prediction of the laser beam degradation was then necessarily limited to average degradation.

The turbulence parameters used to predict the laser beam degradation were the spatial temperature correlation function, spatial velocity correlation function, and the path length of turbulence field thickness associated with each correlation function. The correlation functions actually measured were temporal correlation functions. These functions and Taylor's hypothesis were used to approximate the spatial correlation functions.

Figure 4 shows an example of temperature correlation functions. The time scale equals 33.3 μs. Notice that correlation is imperfect at short time scales. As discussed earlier, the frequency response of the constant current anemometer system, used to measure the temperature perturbations of the turbulent field of this study, was insufficient for many of the flow conditions experienced.

Table 2 lists the rms velocity perturbations, rms measured temperature perturbations, temperature correction factors, corrected rms temperature perturbations, thickness of turbulence field each of these measurements represents, and mean velocity of the flowfield for each of these measurements. The Mach number and downstream test station of each set of parameters is also given.

Predicted vs Measured Unperturbed Laser Beam Far-Field Spot Profiles

In order to compare the unperturbed beam intensity profile actually detected with that which would be analytically predicted, Eq. (11) was numerically integrated with T_r set equal to unity. This yielded the far-field spot in the focal plane of the far-field forming lens. Figures 5a and 5b show the traces of the test beam spots as projected on the opal glass, measured by the TV camera, and portrayed on the oscilloscope. Figures 6a and 6b show the analytically predicted beam spots. As can be seen from the plots, the predicted and measured beam spots were similar for four of the six test beams.

Solution of the Laser Beam Degradation Equations

Equation (11), in combination with Eq. (10), is not amenable to exact solution; thus, numerical techniques were

Table 2 Turbulence parameters

Location Test station	y, cm	Mach no.	u, m/s	θ_s, K	$\sqrt{m}$	θ, K	ΔL, cm	$\bar{U}$, m/s
25	0	0.8	24.0	1.23	1.4	1.72	0.5	156.0
25	0.5	0.8	26.4	1.31	1.4	1.83	1.0	147.0
25	1.0	0.8	29.0	1.35	1.4	1.89	1.0	133.0
25	1.5	0.8	30.8	1.29	1.4	1.81	1.0	114.0
25	2.0	0.8	30.4	1.23	1.3	1.60	1.5	91.8
25	3.0	0.8	25.6	1.09	1.1	1.20	2.0	54.0
25	4.0	0.8	17.6	0.87	1.15	1.00	2.0	27.0
25	5.0	0.8	8.0	0.44	1.1	0.48	2.0	12.4
50	0	0.8	18.4	0.88	1.3	1.15	1.0	112.0
50	1.0	0.8	19.6	0.93	1.4	1.31	2.0	107.0
50	2.0	0.8	21.0	0.91	1.2	1.10	2.0	92.6
50	3.0	0.8	22.2	0.83	1.1	0.92	2.0	77.8
50	4.0	0.8	21.4	0.72	1.1	0.79	2.0	63.4
50	5.0	0.8	19.6	0.62	1.05	0.65	2.0	51.2
50	6.0	0.8	17.4	0.53	1.05	0.55	3.0	38.6
50	8.0	0.8	11.4	0.36	1.0	0.36	4.0	19.4
50	10.0	0.8	5.8	0.26	1.0	0.26	4.0	16.1
75	0	0.8	16.6	0.61	1.0	0.61	2.0	87.6
75	2.0	0.8	17.8	0.62	1.0	0.62	4.0	78.9
75	4.0	0.8	18.4	0.57	1.0	0.57	4.0	65.0
75	6.0	0.8	17.4	0.48	1.0	0.48	4.0	50.8
75	8.0	0.8	15.2	0.38	1.0	0.38	4.0	36.0
75	10.0	0.8	12.7	0.29	1.0	0.29	6.0	25.6
25	0	0.6	19.6	0.77	1.46	1.12	0.5	119.0
25	0.5	0.6	21.0	0.81	1.09	1.0	1.0	112.0
25	1.0	0.6	23.0	0.82	1.3	1.06	1.0	99.4
25	1.5	0.6	23.6	0.79	1.3	1.02	1.0	85.8
25	2.0	0.6	23.0	0.72	1.1	0.79	1.5	70.8
25	3.0	0.6	20.0	0.62	1.05	0.65	2.0	43.1
25	4.0	0.6	13.6	0.26	1.1	0.29	2.0	21.6
25	5.0	0.6	6.8	0.17	1.0	0.17	2.0	8.6
50	0	0.6	15.4	0.54	1.05	0.56	1.0	84.4
50	1.0	0.6	16.6	0.56	1.05	0.58	2.0	81.8
50	2.0	0.6	17.6	0.56	1.0	0.56	2.0	73.2
50	3.0	0.6	17.2	0.50	1.0	0.50	2.0	61.8
50	4.0	0.6	16.4	0.44	1.05	0.46	2.0	50.1
50	5.0	0.6	15.6	0.37	1.0	0.37	2.0	39.4
50	6.0	0.6	13.7	0.31	1.0	0.31	3.0	29.2
50	8.0	0.6	9.5	0.21	1.0	0.21	5.0	16.4
75	0	0.6	12.8	0.38	1.05	0.40	2.0	61.6
75	2.0	0.6	13.4	0.39	1.0	0.39	4.0	56.4
75	4.0	0.6	13.6	0.34	1.0	0.34	4.0	47.6
75	6.0	0.6	12.8	0.28	1.0	0.28	6.0	36.4
75	10.0	0.6	9.5	0.17	1.0	0.17	10.0	17.8
25	0	0.4	13.8	0.43	1.1	0.47	0.5	81.6
25	0.5	0.4	15.2	0.43	1.2	0.51	1.0	76.6
25	1.0	0.4	15.8	0.43	1.2	0.51	1.0	68.4
25	1.5	0.4	16.2	0.41	1.2	0.49	1.0	58.2
25	2.0	0.4	15.8	0.38	1.05	0.4	1.5	48.0
25	3.0	0.4	13.0	0.31	1.05	0.33	2.0	29.6
25	4.0	0.4	9.6	0.23	1.1	0.25	2.0	16.5
25	5.0	0.4	5.0	0.17	1.0	0.17	2.0	7.3
50	0	0.4	11.0	0.29	1.1	0.32	1.0	60.8
50	1.0	0.4	11.8	0.30	1.1	0.33	2.0	57.5
50	2.0	0.4	12.4	0.30	1.0	0.30	3.0	49.6
50	4.0	0.4	11.6	0.23	1.0	0.23	4.0	35.1
50	6.0	0.4	9.4	0.23	1.0	0.23	6.0	21.4
75	0	0.4	9.2	0.25	1.0	0.25	2.0	41.1
75	2.0	0.4	9.6	0.24	1.0	0.24	4.0	39.2
75	4.0	0.4	8.8	0.23	1.1	0.25	4.0	31.8
75	6.0	0.4	8.8	0.20	1.05	0.21	6.0	26.4
75	10.0	0.4	6.3	0.16	1.0	0.16	10.0	13.6

resorted to in an endeavor to solve these equations. Simpson's rule was used to integrate numerically the equations with "Δr" of 0.125 mm. In order to utilize conveniently the temperature and velocity correlation functions in the numerical integrations, the correlation functions were digitized using a least-squares fit subroutine. The results of the numerical integration of this equation are shown in Table 3. Solutions were obtained for measured input laser beam diameters.

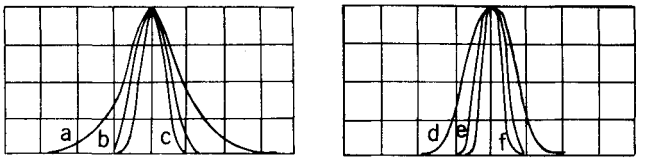

Fig. 5 Measured beam images. 6328 Å: a) 11 mm beam; b) 26.8 mm beam; c) 50 mm beam; 4416 Å: d) 12.3 mm beam; e) 26 mm beam; f) 50 mm beam.

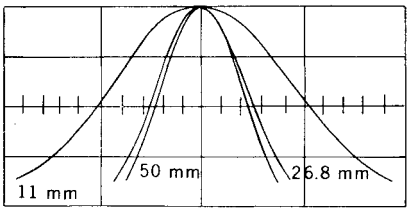

6328 Å

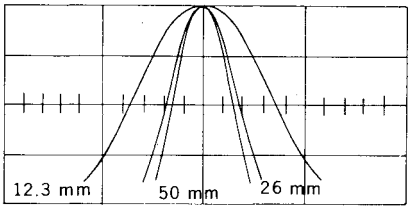

4416 Å

Fig. 6 Calculated beam images.

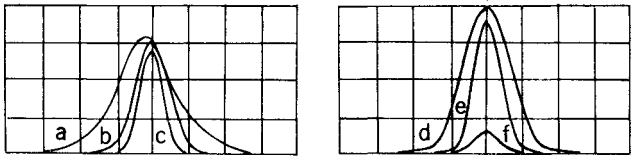

Fig. 7 Degraded beam images. 6328 Å: a) 11 mm, Mach 0.8, 50 cm station; b) 26.8 mm, Mach 0.6, 25 cm station; c) 50 mm, Mach 0.6, 25 cm station; 4416 Å: d) 12.3 mm, Mach 0.4, 50 cm station; e) 26 mm, Mach 0.6, 75 cm station; f) 50 mm, Mach 0.8,, 25 cm station.

Predicted vs Measured Turbulent Refractive Index-Induced Laser Beam Degradations

Examples of the degraded far-field laser beam spots, as recorded on the oscilloscope, are shown in Fig. 7. These photographs show the long-term average degraded laser beam spots, as measured by the TV camera in the regular scan mode. Since these examples show little motion of the far-field spot, it is apparent that any motion which contributes to the overall degradation, occurs at a frequency equal to or higher than the reciprocal of the integration time of the TV camera system. This frequency of motion will be discussed further when the results of the far-field measurements using the TV camera in the single-line scan mode are presented. Figure 8 shows the percentage of the detected long-term average central spot intensities at the 25 cm station for all laser beams and Mach numbers. Table 3 lists these same data along with the solution of Eq. (11) using Eq. (10) for T_τ. Figure 9 shows in graphical form the detected far-field spot intensities versus those predicted by the solution of Eq. (11) using Eq. (10) for T_τ with input beam diameters that would yield the far-field spot diameters measured.

Table 3 Measured and calculated laser beam degraded intensities

λ, Å	Laser beam size, mm	Mach no.	Test station, cm	Measured intensity, %	Calculated intensity, % Eq. (10)	λ, Å	Laser beam size, mm	Mach no.	Test station, cm	Measured intensity, %	Calculated intensity, % Eq. (10)
6328	50.0	0.4	25	93	92.8	4416	26.0	0.6	50	81	74.2
6328	26.8	0.4	25	94	93.6	4416	12.3	0.6	50	89	86.6
6328	11.0	0.4	25	98	96.9	4416	21.0	0.6	50	81	77.1
4416	50.0	0.4	25	90	85.8	4416	10.8	0.6	50	89	88.7
4416	26.0	0.4	25	92	87.6	6328	50.0	0.8	50	60	60.7
4416	12.3	0.4	25	97	92.9	6328	26.8	0.8	50	68	65.6
4416	21.0	0.4	25	92	88.8	6328	11.0	0.8	50	85	83.9
4416	10.8	0.4	25	97	93.9	4416	50.0	0.8	50	41	38.2
6328	50.0	0.6	25	70	72.8	4416	26.0	0.8	50	51	45.2
6328	26.8	0.6	25	76	75.8	4416	12.3	0.8	50	72	67.3
6328	11.0	0.6	25	86	87.7	4416	21.0	0.8	50	51	50.0
4416	50.0	0.6	25	56	53.1	4416	10.8	0.8	50	72	71.5
4416	26.0	0.6	25	63	58.1	6328	50.0	0.4	75	97	96.9
4416	12.3	0.6	25	79	74.2	6328	26.8	0.4	75	98	97.4
4416	21.0	0.6	25	63	61.6	6328	11.0	0.4	75	100	99.0
4416	10.8	0.6	25	79	77.3	4416	50.0	0.4	75	98	93.8
6328	50.0	0.8	25	34	40.6	4416	26.0	0.4	75	97	94.9
6328	26.8	0.8	25	45	46.0	4416	12.3	0.4	75	99	97.7
6328	11.0	0.8	25	67	69.1	4416	21.0	0.4	75	97	95.6
4416	50.0	0.8	25	18	18.6	4416	10.8	0.4	75	99	98.1
4416	26.0	0.8	25	25	24.2	6328	50.0	0.6	75	91	90.6
4416	12.3	0.8	25	48	45.4	6328	26.8	0.6	75	92	92.0
4416	21.0	0.8	25	25	28.4	6328	11.0	0.6	75	98	96.9
4416	10.8	0.8	25	48	50.4	4416	50.0	0.6	75	83	81.8
6328	50.0	0.4	50	96	95.3	4416	26.0	0.6	75	87	84.8
6328	26.8	0.4	50	97	96.0	4416	12.3	0.6	75	94	92.7
6328	11.0	0.4	50	98	98.4	4416	21.0	0.6	75	87	86.7
4416	50.0	0.4	50	94	90.7	4416	10.8	0.6	75	94	93.9
4416	26.0	0.4	50	95	92.1	6328	26.8	0.8	75	80	78.6
4416	12.3	0.4	50	98	96.2	6328	50.0	0.8	75	74	75.0
4416	21.0	0.4	50	95	93.0	6328	11.0	0.8	75	90	91.1
4416	10.8	0.4	50	98	96.8	4416	50.0	0.8	75	57	56.6
6328	50.0	0.6	50	83	83.6	4416	26.0	0.8	75	65	62.7
6328	26.8	0.6	50	86	86.0	4416	12.3	0.8	75	81	80.4
6328	11.0	0.6	50	95	94.1	4416	21.0	0.8	75	65	66.9
4416	50.0	0.6	50	78	69.8	4416	10.8	0.8	75	81	83.3

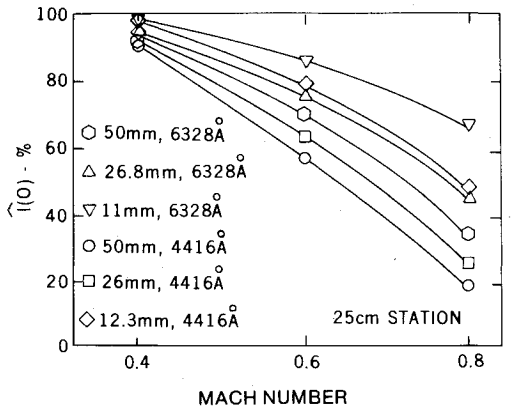

Fig. 8 Average degraded intensities.

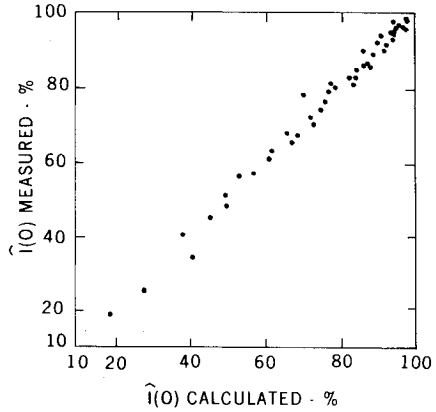

Fig. 9 Measured vs calculaed intensities.

Laser Beam Far-Field Spot Broadening and Wandering

With the TV camera in the single-line scan mode, the detection system was able to detect motions with a frequency up to 3000 Hz. Examples were made of several measurements of the beam spots with the TV camera in the single-line scan mode and with several detected spots superimposed. The maximum intensity recorded was taken as the intensity remaining after degradation by broadening alone. The percentage of this maximum, which yields the long-term average intensity, was taken as the intensity remaining after degradation by beam motion (or wandering) alone. Table 4 lists these percentages for all test conditions.

V. Summary and Conclusions

This investigation correlated the degradation of the far-field central spot intensity formed by a collimated coherent light beam traversing high-intensity turbulence with the statistical behavior of the turbulence-generated refractive index perturbations causing the degradation. Since refractive index perturbations could not be measured readily, a method to approximate these perturbations, via the equation of state, using velocity and temperature perturbations was autocorrelated. The turbulence quantities measured were path length, velocity correlation function, and temperature correlation function. The path length had a minimum at the

Table 4 Laser beam wandering vs broadening

		λ(Å), beam size, mm					
		6328			4416		
		50.0	26.8	11.0	50.0	26.0	12.3
25 cm test station							
0.4 Mach	I	99	99	100	100	100	99
	$\bar{I}$	93	94	98	90	92	97
	%	94	95	98	90	92	98
0.6 Mach	I	80	91	95	77	83	92
	$\bar{I}$	70	76	86	56	63	79
	%	88	84	91	73	76	86
0.8 Mach	I	55	65	75	28	40	65
	$\bar{I}$	34	45	67	18	25	48
	%	62	69	90	64	63	74
50 cm test station							
0.4 Mach	I	99	99	99	100	100	100
	$\bar{I}$	96	97	98	94	95	98
	%	97	98	99	94	95	98
0.6 Mach	I	92	96	98	95	95	98
	$\bar{I}$	83	86	95	78	81	89
	%	90	90	97	82	85	91
0.8 Mach	I	80	86	94	70	82	90
	$\bar{I}$	60	68	85	41	51	72
	%	75	79	90	59	62	80
75 cm test station							
0.4 Mach	I	100	100	100	100	100	100
	$\bar{I}$	97	98	100	98	97	99
	%	97	98	100	98	97	99
0.6 Mach	I	100	99	99	100	100	100
	$\bar{I}$	91	92	98	83	87	94
	%	91	93	99	83	87	94
0.8 Mach	I	90	94	95	96	96	96
	$\bar{I}$	74	80	90	57	65	81
	%	82	85	95	59	68	84

25 cm test station of about 10 cm, and a maximum of about 30 cm at the 75 cm test station. The rms velocity perturbations had a maximum of 30.8 m/s at the 25 cm test station at 0.8 Mach and an on-axis minimum of 9.2 m/s at the 75 cm test station at 0.4 Mach. The corrected temperature perturbations had a maximum of 1.89 K and minimum of 0.25 K at the preceding respective test stations and nozzle exit flow conditions.

The actual far-field central spot intensities were measured. The 4416 Å, 50 mm beam traversing the 25 cm test station when the nozzle exit velocity was 0.8 Mach, had an intensity of 18% of the reference intensity. At the 75 cm test station, with 0.4 Mach nozzle exit velocity, the 6328 Å, 11.0 mm laser beam had a far-field central spot intensity of 100% of the reference intensity.

The results of the experimentally measured central spot degraded intensities were compared with those that were analytically predicted using experimentally determined turbulence characteristics (Fig. 9). For the same laser beams traversing statistically identical flowfields, the greatest difference between experimentally measured and analytically predicted degraded far-field, central spot intensities was 8.2%. The average difference between the experimentally and analytically determined intensities for all test conditions was less than 2%. These results support the approximations used to arrive at the analytical expressions which predict the laser beam far-field central spot intensity degradation caused by turbulent flowfields, and yield confidence in the ability to accurately predict those degradations using readily measurable turbulent flowfield statistical parameters.

VI. References

[1] Hufnagle, R. E and Stanley, N. R., "Modulation Transfer Function Associated with Image Transmission Through Turbulent Media," *Journal of the Optical Society of America*, Vol. 54, No. 1, 1964.

[2] Lutomirski, R. F., Huschke, R. E., Meecham, W. C., and Yura, H. T., "Degradation of Laser Systems by Atmospheric Turbulence," R-1171-ARPA/RC, The Rand Corp., June 1973.

[3] Lutomirski, R. F., Shapiro, A. R., and Yura, H. T., "Experiments on Turbulence Effects in Laser Propagation," WN-7063-ARPA, The Rand Corp., Sept. 1970.

[4] Lutomirski, R. F. and Yura, H. T., "Wave Structure Function and Mutual Coherence Function of an Optical Wave in a Turbulent Atmosphere," *Journal of the Optical Society of America*, Vol. 61, 1971, p. 482.

[5] Sutton, G. W., "Effect of Turbulent Fluctuations in an Optically Active Fluid Medium," *AIAA Journal*, Vol. 7, Sept. 1969, p. 1751

[6] Tatarski, V. I., *Wave Propagation in Turbulent Medium*, McGraw-Hill Book Co., New York, N.Y., 1961.

[7] Owens, J. C., "Optical Refractive Index of Air: Dependence on Pressure, Temperature and Composition," *Applied Optics*, Vol. 6, Jan. 1967, p. 51.

[8] Cudahy, G. F., "An Investigation of the Degradation of a Laser Beam by High Intensity Turbulence," Ph.D. Thesis, Air Force Institute of Technology, 1976.

[9] Corrsin, S. and Uberoi, M. S., "Spectra and Diffusion in a Round Turbulent Jet," NACA Rept. 1040, U.S. Government Printing Office, 1951.

[10] Hinze, J. O., *Turbulence*, McGraw-Hill Book Co., Inc., New York, N.Y., 1959.

[11] Shepard, W. K., "Turbulence Measurements in Plane Free Jet at High Subsonic Velocities," GAE/AE/74D-24, Air Force Institute of Technology, Air University, Wright-Patterson AFB, Ohio, 1974.